

Electronic Supplementary Information for:

Improving charge collection with delafossite photocathodes: a Host-Guest $\text{CuAlO}_2/\text{CuFeO}_2$ approach

Mathieu S. Prévot,^a Yang Li,^{a,b} Néstor Guijarro,^a and Kevin Sivula^{a*}

^aLaboratory for Molecular Engineering of Optoelectronic Nanomaterials, École Polytechnique Fédérale de Lausanne (EPFL), Station 6, 1015 Lausanne, Switzerland.

^bCollaborative Innovation Center of Chemical Science and Engineering (Tianjin), Tianjin Key Laboratory of Applied Catalysis Science and Technology, State Key Laboratory of Chemical Engineering (Tianjin University), School of Chemical Engineering, Tianjin University, Tianjin 300072, China.

*Email: kevin.sivula@epfl.ch

X-Ray Photoelectron Spectroscopy

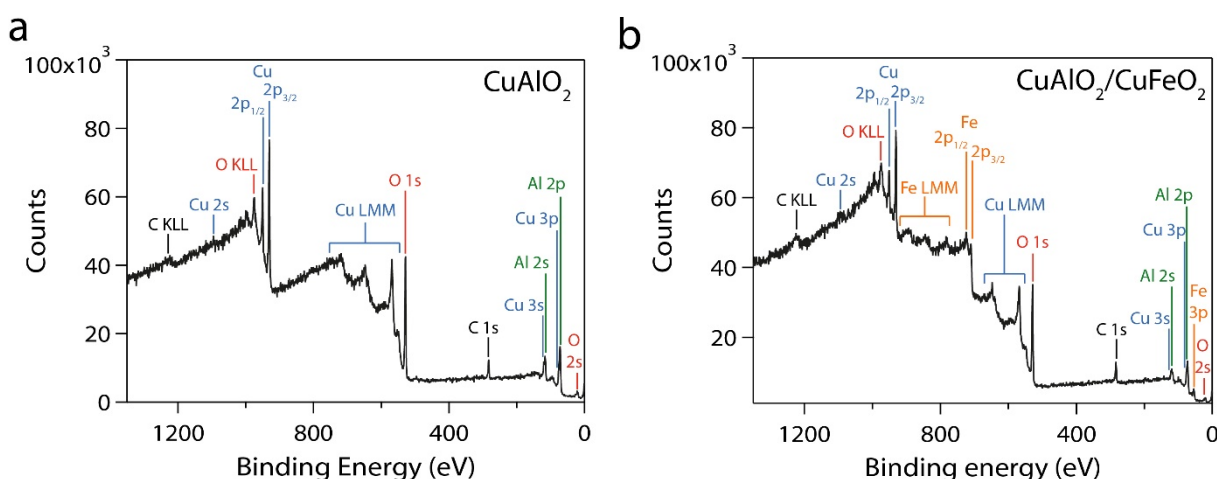


Figure S1 XPS spectra of a CuAlO_2 thin film (a) and a $\text{CuAlO}_2/\text{CuFeO}_2$ thin film (b). The peaks were attributed using the database of the PHI Multipak software (Ulvac-Phi, Inc.).

Band gap determination

UV-vis spectroscopy was used to determine the optical band gaps of the materials. We used an integrating sphere to measure the diffuse reflectance spectra of the scattering films (CuAlO_2 and $\text{CuAlO}_2/\text{CuFeO}_2$) or the absorption spectrum of the transparent CuFeO_2 film. We then used the Kubelka-Munk transformation to extract $F(R)$, proportional to the absorption coefficient α , for the scattering films, while the absorption coefficient of bare CuFeO_2 was calculated from the absorbance and the thickness z of the film:

$$\alpha = \frac{A \ln 10}{z}$$

Finally the following relationship was used:

$$(\alpha h\nu)^n \propto (h\nu - E_g^{opt})$$

where $h\nu$ is the photon energy, E_g^{opt} the optical band gap, and $n=2$ (direct transition) or $n=1/2$ (indirect transition). The band gap is extracted by plotting $(\alpha h\nu)^n$ or $(F(R)h\nu)^n$ vs $h\nu$, and taking the intercept of the linear part of the curve with the x-axis. We obtained a direct band gap of 3.51 eV for CuAlO_2 , and an indirect band gap of 1.45 eV for CuFeO_2

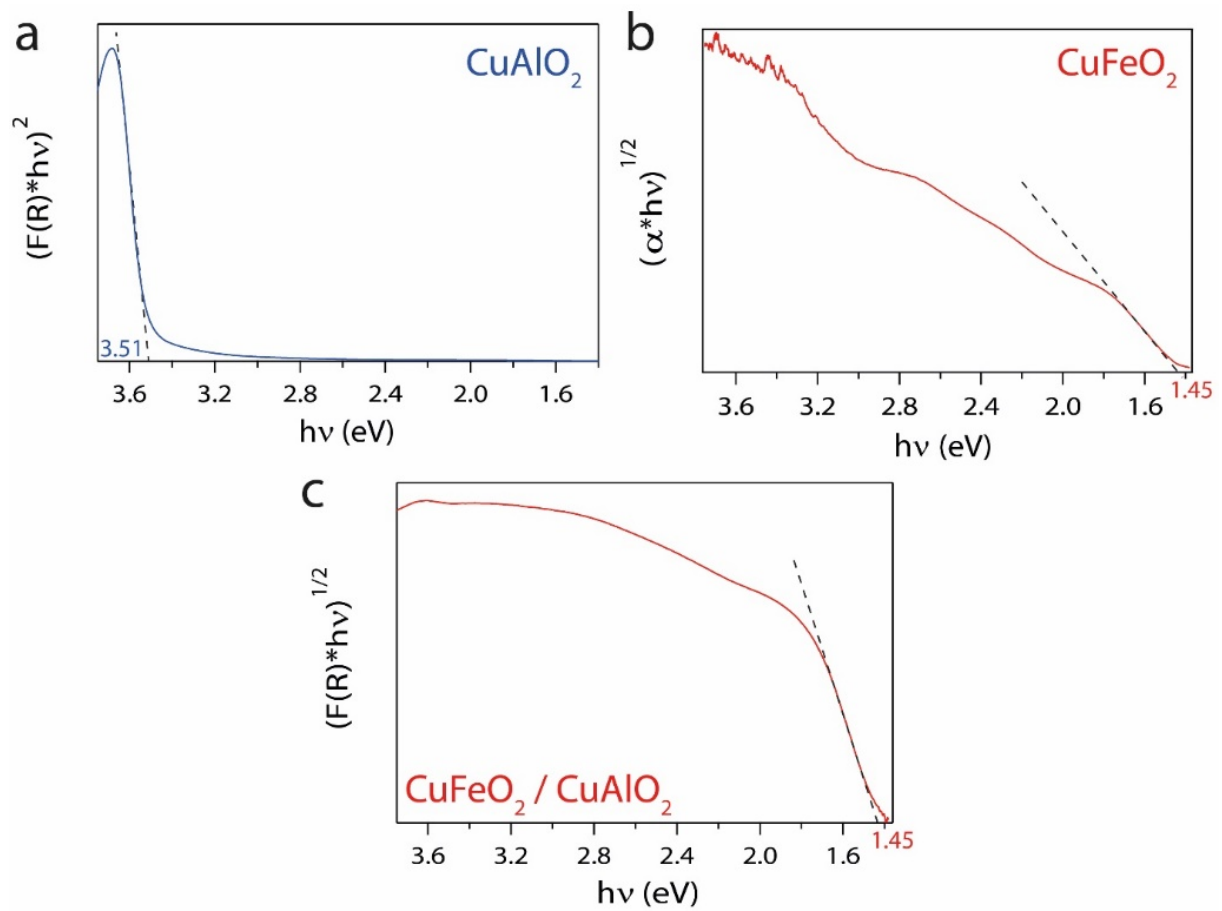


Figure S2 Tauc plots of the CuAlO_2 scaffold (a), a bare CuFeO_2 film (b) and a $\text{CuFeO}_2/\text{CuAlO}_2$ electrode (c)

Additional Scanning electron micrographs

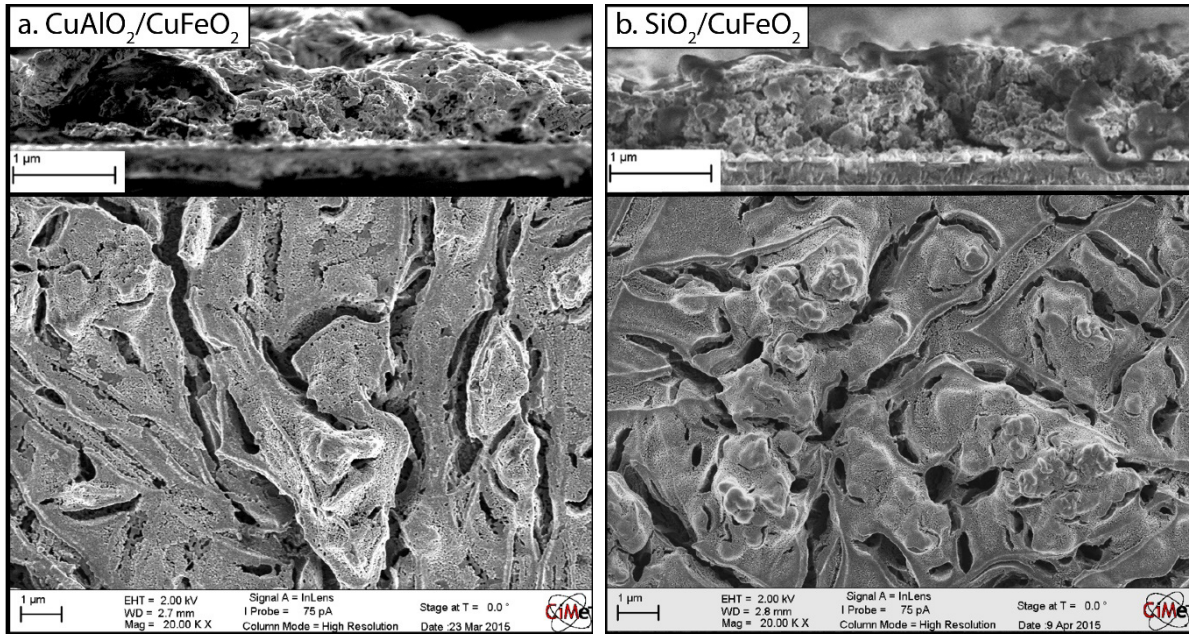


Figure S3 a) Cross-sectional and top views of a $\text{CuAlO}_2/\text{CuFeO}_2$ composite electrode. b) Cross-sectional and top views of a $\text{SiO}_2/\text{CuFeO}_2$ composite electrode

Incident photon-to-current efficiency (IPCE) measurement

Integrated photocurrents were calculated using the following formula:

$$J_{ph}(\lambda) = \int_{350 \text{ nm}}^{\lambda} IPCE(\lambda) * N_{ph}(\lambda) d\lambda$$

where $N_{ph}(\lambda)$ is the number of photons emitted under AM1.5 illumination at a wavelength λ .

Mott-Schottky analysis

The Mott-Schottky equation was used to extract the Flat-band potential from the Mott-Schottky plots:

$$\frac{1}{C^2} = -\frac{2}{e\epsilon\epsilon_0 N_A A^2} \left(E - E_{FB} + \frac{kT}{e} \right)$$

where C is the space charge capacitance, e is the elementary charge, ϵ is the dielectric constant of the material, ϵ_0 is the vacuum permittivity, N_A is the majority carrier density, A is the surface area of the sample, E is the potential of the electrode, E_{FB} is the flat-band potential of the material, k is the Boltzmann constant and T is the absolute temperature. From this equation and the data graphed in Figure 3a, we measured

Additional J-V curve

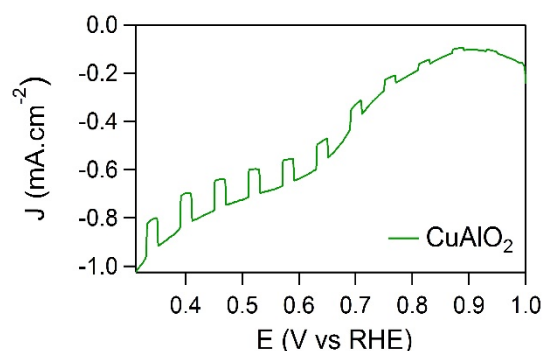


Figure S4 J-V curves of a 2 μm CuAlO₂ film on FTO, under O₂ bubbling. Electrolyte: 1M NaOH, scan rate: 10 mV.s⁻¹, under 1 sun illumination

Thickness optimization

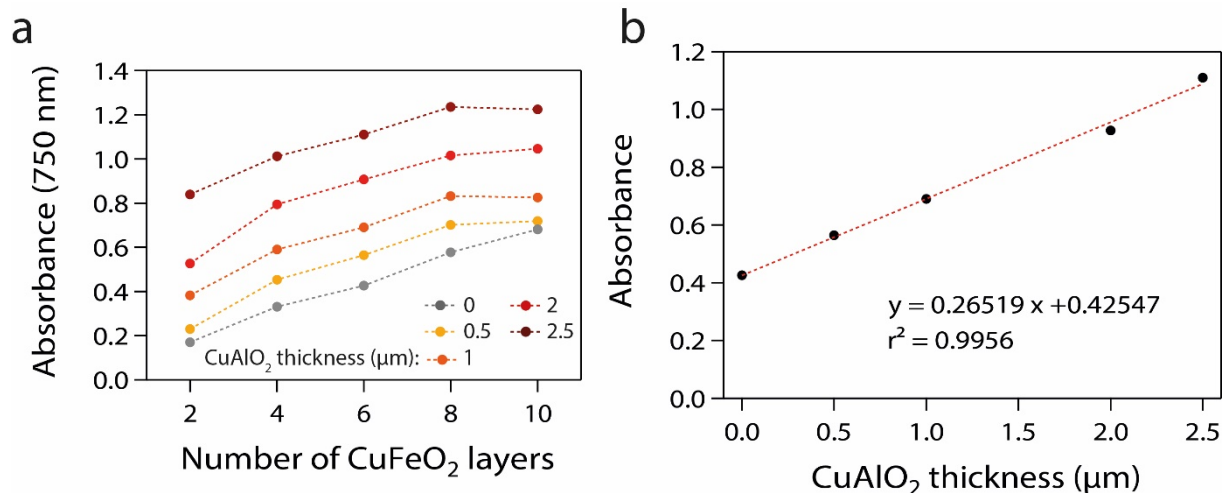


Figure S5. a) Absorbance of the same electrodes at 750 nm. b) Dependence of the absorbance of composite electrodes made with 6 successive depositions of CuFeO₂ as a function of the scaffold thickness.

Composite CuAlO₂/CuFeO₂ electrodes of different thicknesses were investigated in a photoelectrochemical setup, containing a 1M NaOH electrolyte purged with O₂, under front (electrolyte-side) and back (substrate-side) illumination. Photocurrents generated at 0.4 V vs RHE were used as a benchmark and are gathered in Figure S4a.

Moreover, the amount of CuFeO₂ in each electrode was estimated using the absorbance of the film at 750 nm (Figure S4b). The absorbance, and therefore the amount of CuFeO₂, of electrodes made with 6 successive deposition of CuFeO₂ was found to depend linearly on the

scaffold thickness (Figure S4c). The absorbance was calculated using the following formula, where the reflected light is removed from the incident beam:

$$A = -\log\left(\frac{I_T}{I_0 - I_R}\right) = -\log\left(\frac{T(\%)}{100 - R(\%)}\right) \propto \text{Amount of CuFeO}_2$$

Additional UV-vis data

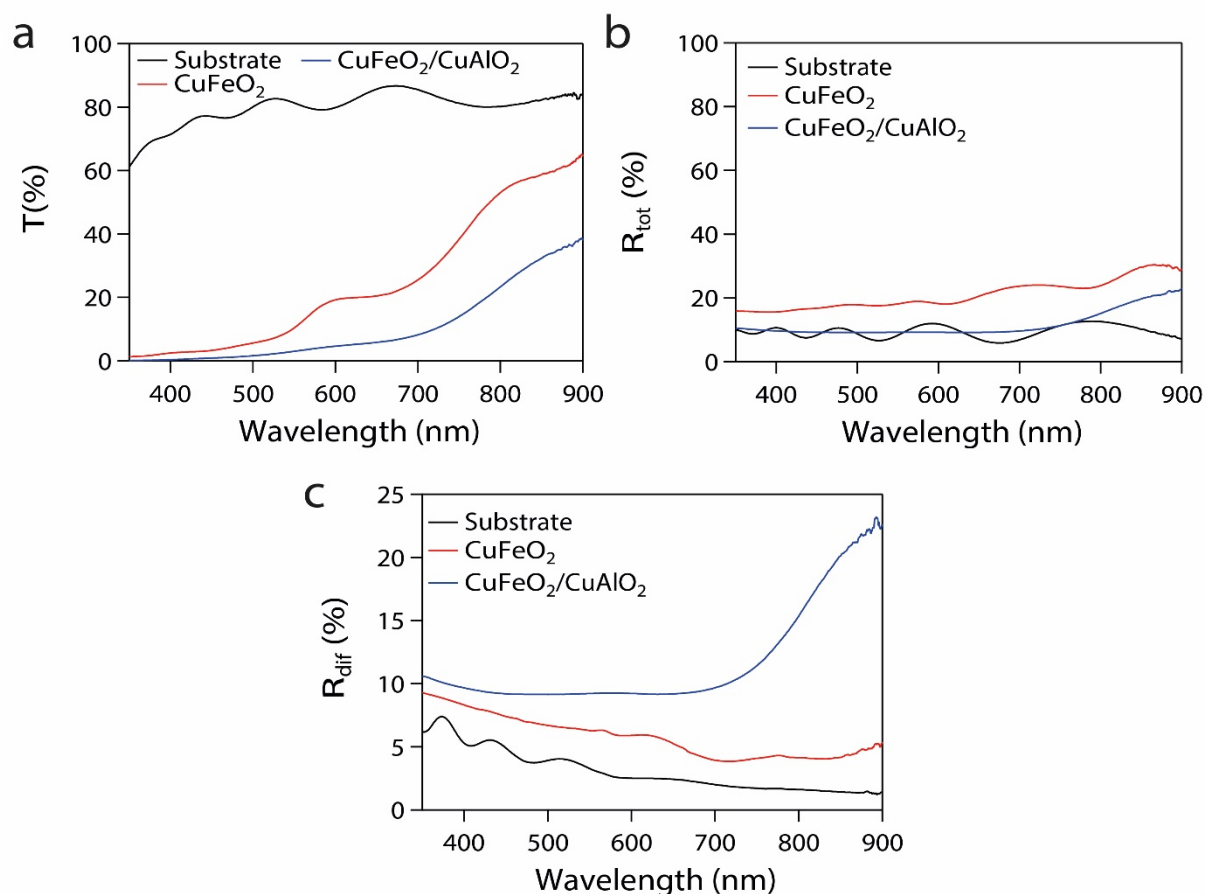


Figure S6 Transmission (a), total reflectance (b) and diffuse reflectance (c) spectra of the substrate (black trace), the bare CuFeO₂ electrode (red trace) and the CuFeO₂/CuAlO₂ electrode (blue trace)

Normalized Quantum Efficiency

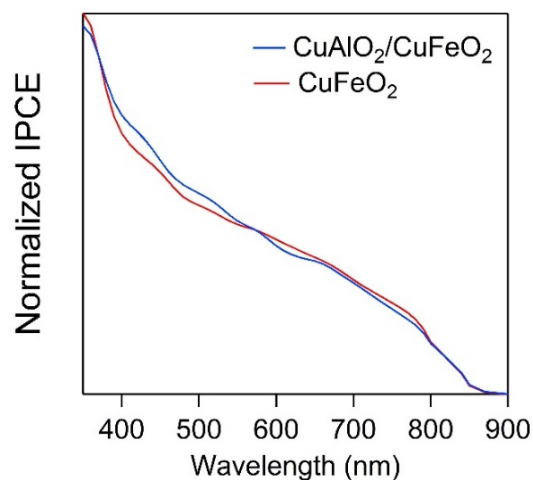


Figure S7 IPCE spectra of the control CuFeO₂ electrode and the composite CuAlO₂/CuFeO₂ electrode, normalized to the same value at 400 nm

Xenon arc lamp calibration

The shape of the lamp spectrum was recorded using an OceanOptics optics USB2000+XR1 ES spectrometer with a Spectralon cosine corrector, which provided a relative measure of the number of photons irradiated by the lamp at each wavelength. This spectrum was adjusted for the AM 1.5 spectrum, so that, when integrated between 300 nm and 850 nm, both spectra gave the same number of photons, as shown in Fig. S9. The calibrated spectrum corresponds to the spectrum of the Xenon arc lamp providing as many photons as the AM 1.5 spectrum between 300 nm and 850 nm.

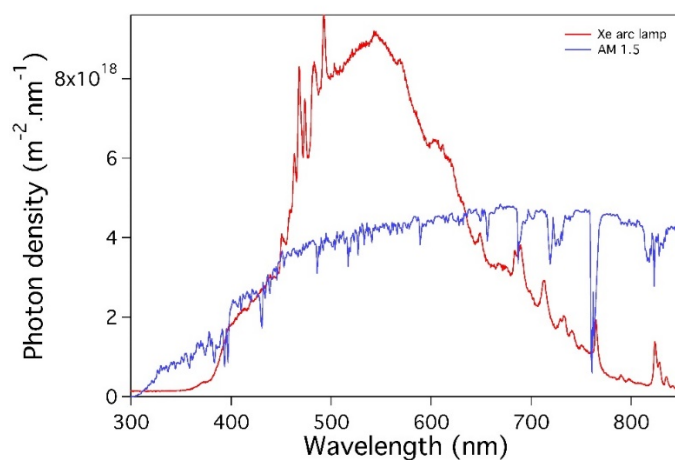


Figure S8 Xe arc lamp emission spectrum (red line) calibrated with the solar AM 1.5 spectrum (blue line) for the number of incident photons between 300 nm and 850 nm

Reduction reaction mechanism proposal.

In this study, we used oxygen as an electron scavenger so that the electrochemical reaction was not the limiting part of the photoelectrochemical process. Under these conditions, a modification in the photocurrent produced by the electrode has to come from a modification of the charge transport/separation inside the semiconductor. It was therefore a useful tool to characterize the improvements brought by the introduction of the CuAlO₂ underlayer.

While oxygen reduction would not be the ultimate purpose of our photocathode, the mechanism is not of fundamental importance in this work. However, we propose here some clues on a possible mechanism. We used 4-nitrophenylboronic acid, a molecule that oxidizes in the presence of H₂O₂ or HO₂⁻ (its conjugated base) and yields a colored species, with an absorption peak at 400 nm vs. 300 nm for the reduced form (*American Journal of Analytical Chemistry*, 2011, **2**, 879-884). When oxygen was reduced at the surface of our photocathode, we observed an increase in the absorption of the solution at 400 nm over time (see Figure S9), suggesting that HO₂⁻ was likely produced as a result of the reduction of O₂.

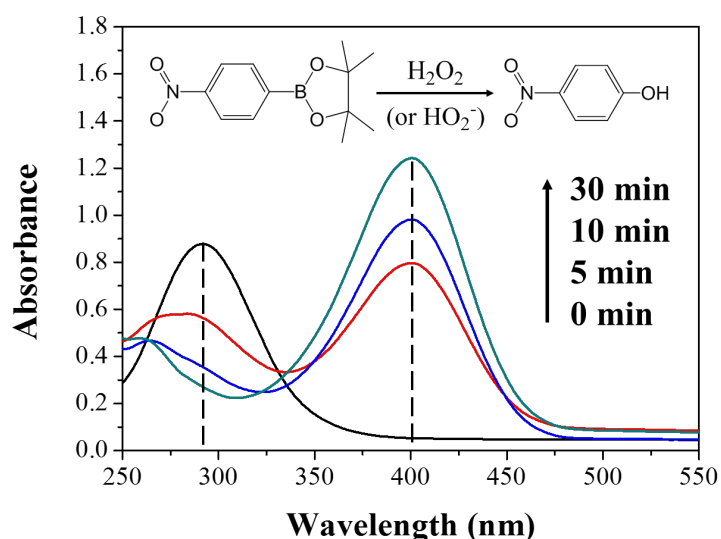
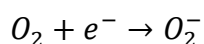
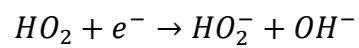
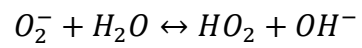


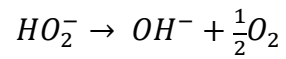
Figure S9. UV-Vis absorption spectra of 100 μM 4-nitrophenyl boronic acid pinacol ester before and after photoelectrochemical oxygen reduction reaction (20 mM Tris buffer, pH 10.0).

We therefore propose the following mechanism in basic medium (see B.H.J. Bielski et al. *J. Phys. Chem. Ref. Data*. **1985**, *14*, 1041) :

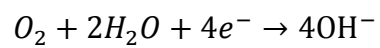




As HO_2^- is a peroxide species, known to be unstable it then probably decomposes to yield water and oxygen



The overall reaction is therefore summarized by:



i.e. the oxygen reduction reaction in aqueous basic conditions.